Mod Rheumatol (2010) 20:11–17
DOI 10.1007/s10165-009-0224-7

ORIGINAL ARTICLE

Correlation between MMP-13 and HDAC7 expression in human knee osteoarthritis

Reiji Higashiyama · Shigeru Miyaki · Satoshi Yamashita · Teruhito Yoshitaka · Görel Lindman · Yoshiaki Ito · Takahisa Sasho · Kazuhisa Takahashi · Martin Lotz · Hiroshi Asahara

Received: 3 April 2009 / Accepted: 5 August 2009 / Published online: 26 September 2009

Abstract Recent studies suggest that histone deacetylase (HDAC) inhibitors may therapeutically prevent cartilage degradation in osteoarthritis (OA). Matrix metalloproteinase-13 (MMP-13) plays an important role in the pathogenesis of this disease and in the present study we investigated the correlation between HDACs and MMP-13. Comparing the expression of different HDACs in cartilage from OA patients and healthy donors, HDAC7 showed a significant elevation in cartilage from OA patients. High level of HDAC7 expression in OA cartilage was also confirmed by immunohistochemistry. Knockdown of HDAC7 by small interference RNA (siRNA) in SW1353 human chondrosarcoma cells strongly suppressed interleukin (IL)-1-dependent and independent induction of MMP-13 gene expression. In conclusion, elevated HDAC7 expression in human OA may contribute to cartilage degradation via promoting MMP-13 gene expression, suggesting the critical role of MMP-13 in OA pathogenesis.

Keywords Osteoarthritis · HDAC7 and MMP-13

R. Higashiyama · S. Miyaki · M. Lotz · H. Asahara
Division of Arthritis Research, The Scripps Research Institute, 10550 North Torrey Pines Road, La Jolla, CA 92037, USA

R. Higashiyama · S. Yamashita · T. Yoshitaka · G. Lindman · Y. Ito · H. Asahara (✉)
Department of Systems BioMedicine, National Research Institute for Child Health and Development, 2-10-1 Okura, Setagaya, Tokyo 157-8535, Japan
e-mail: asahara@nch.go.jp

R. Higashiyama · T. Sasho · K. Takahashi
Department of Orthopaedic Surgery, Graduate School of Medicine, Chiba University, Chiba, Japan

Abbreviations

MMP	Matrix metalloproteinase
OA	Osteoarthritis
HDAC	Histone deacetylase
RT-PCR	Reverse-transcriptase polymerase chain reaction
IL-1	Interleukin-1β
TSA	Trichostatin A

Background

Osteoarthritis (OA) is a chronic degenerative joint disorder and a major cause of disability in the elderly. Characterized by progressive structural changes in articular cartilage, with persistent degeneration the disease eventually leads to loss of joint function. A significant feature of OA is excessive production of inflammatory mediators [1–3], among which pro-inflammatory cytokine interleukin-1β (IL-1) plays a crucial role in the pathophysiology. IL-1 induces a cascade of inflammatory and catabolic events in chondrocytes, changing chondrocyte anabolism through suppression of proteoglycan and collagen synthesis and by enhancing matrix metalloproteinase (MMP) production.

Several lines of evidence suggest that MMP-13 contributes to cartilage degradation in OA. MMP-13 expression is significantly higher in chondrocytes from cartilage of late-stage OA compared with early OA or normal knee cartilage [4]. In explant cultures treated with a specific MMP-13 inhibitor, release of collagen degradation products from human OA cartilage is reduced [5]. Furthermore, transgenic mice overexpressing activated MMP-13 in the articular chondrocytes develop joint degradation similar to human OA [6]. Characterization of MMP-13 expression

regulation in articular chondrocytes will contribute to understanding the molecular etiology of OA.

Two families of histone deacetylase (HDACs) have been identified: the classical HDAC family and the NAD^+-dependent, so-called SIR2 family (sometimes called class III HDACs). Classical HDACs can be grouped into 3 classes (I, II, and IV) based on phylogeny [7]. Class I HDACs (HDAC1, 2, 3, and 8) are related to yeast RPD3, and class II HDACs (HDAC4, 5, 6, 7, 9, and 10) are more closely related to yeast HDA1 [8]. HDAC11 alone represents class IV, and HDAC11-related proteins have been described in all eukaryotic organisms with the exception of fungi [7]. Trichostatin A (TSA) is a HDAC inhibitor [8] with a broad spectrum of activity against class I and II HDACs, but not HDACs from the SIR2 family. Administration of these reagents to cells blocks histone deacetylation and leads to increased histone acetylation within gene expression in susceptible genes. There are also, however, many cases in which HDAC inhibitors act as repressors of gene expression [9–13].

Recently, HDACs have emerged as targets in cancer therapy and inflammatory diseases, including rheumatoid arthritis (RA) and OA [14–23], but it is still unclear which HDACs are specifically involved in cartilage degradation. These observations prompted us to investigate HDAC expression in normal and OA cartilage and identify the specific HDAC that contributes to cartilage degradation in human OA.

Materials and methods

Cartilage procurement and processing

Cartilage was obtained from 6 normal donors (age range 19–49 years; Mankin score 0–2 points) and 10 OA donors (age range 44–93 years; Mankin score 5–10 points). All tissue samples were graded according to a modified Mankin scale [24], for which <3 points was normal and ≥5 points represented OA. Normal articular cartilage was harvested from femoral condyles and tibial plateaus of human tissue donors under approval from the Scripps Human Subjects Committee. Osteoarthritis cartilage was obtained from patients undergoing knee replacement surgery. Cartilage thickness ranged from 1.5 to 2.8 mm. Cartilage surfaces were rinsed with saline and parallel sections 5 mm apart were cut vertically from the cartilage surface onto subchondral bone with a scalpel. These cartilage strips were then resected from bone. Human chondrocytes were isolated and cultured as previously described [25]. Cartilage tissue was incubated with trypsin at 37°C for 10 min. Following removal of trypsin solution, tissue slices were treated for 12–16 h with type IV clostridial collagenase in Dulbecco's modified Eagle's medium (DMEM) with 5% fetal calf serum. After initial isolation, cells were kept in high-density cultures in DMEM (high glucose) supplemented with 10% CS, L-glutamine, and antibiotics and allowed to attach to the surface of the culture flasks. After cells had grown to confluence, they were split once (passage 1) and grown to confluence again in preparation for experiments [26].

Cell culture

Human knee chondrocytes were grown to confluence in 35-mm 6-well plates with 2 mL DMEM containing 10% CS with or without TSA (SIGMA Inc.) at 300 nM for 24 h (Fig. 1a). In parallel, cells were precultured for 5 h with 5 ng/mL IL-1, after which TSA was added at 300 nM and cultured additionally 24 h (Fig. 1b).

Knockdown experiments by small interference RNA (siRNA) were carried out on SW1353 human chondrosarcoma cells transfected with 25 nmol siHDAC7 (Applied Biosystems Inc.) using Lipofectamine 2000 (Invitrogen Corporation) for 5 h, following the manufacturer's instructions. Then incubation with 5 ng/mL IL-1 was done. In preliminary experiments, we could knock down the HDAC7 expression level to 20% by 25 nmol siHDAC7. Because the siHDAC7 effect was not enough in human

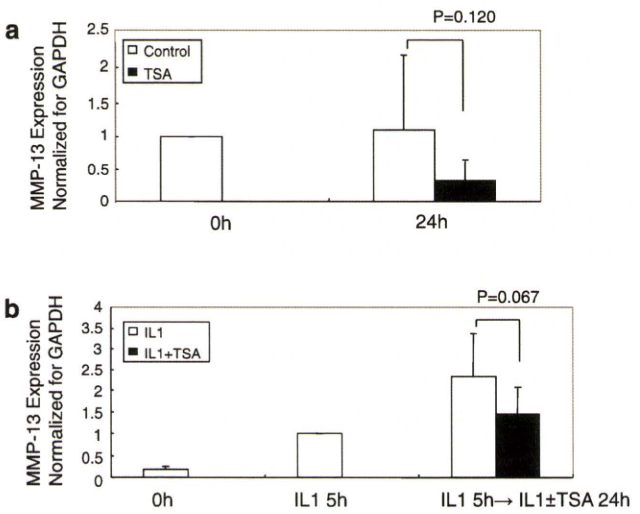

Fig. 1 TSA suppresses both natural and IL-1-induced MMP-13 expression. TSA lowered both natural and IL-1-induced MMP-13 expression, although the effect was not statistically significant. Real-time PCR results from **a** human knee chondrocytes ($n = 6$, age range 19–66 years) treated or untreated with 300 nM TSA for 24 h, and **b** chondrocytes stimulated with IL-1 (5 ng/mL) for 5 h and then treated or untreated with TSA (300 nM) for 24 h. GAPDH gene expression was used for normalization. Results are expressed as fold changes relative to a value of 1 for untreated control cells. $P = 0.120$ (**a**). Results are expressed as fold changes relative to a value of 1 for untreated control cells after 5 h of IL-1 stimulation. $P = 0.067$ (**b**)

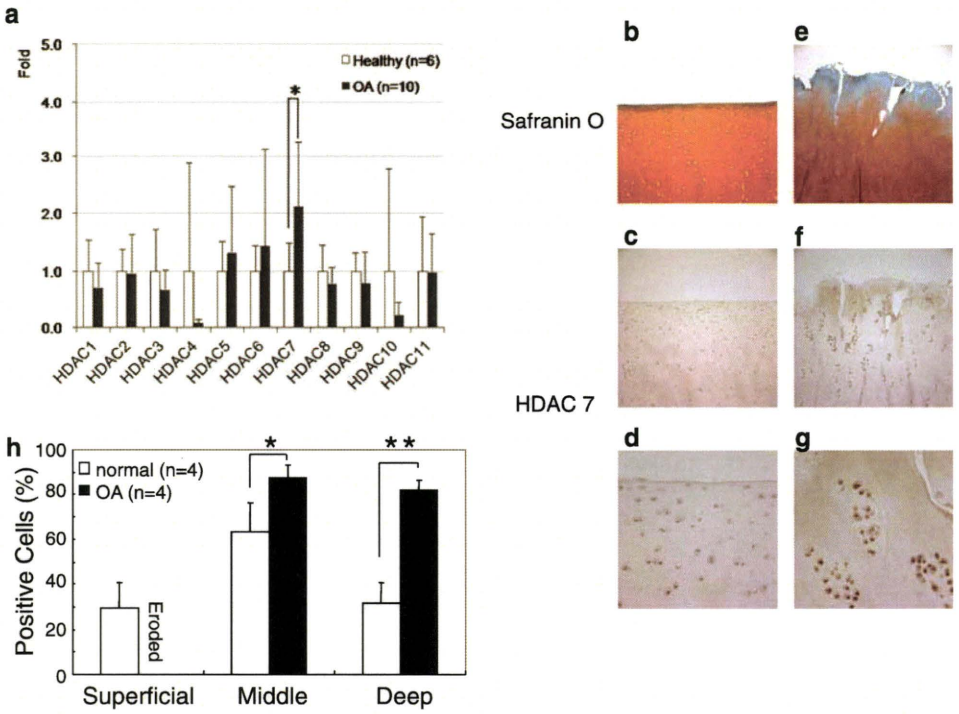

Fig. 2 Localization of HDAC7 in normal and OA knee cartilage. **a** HDAC1–11 mRNA expression in human knee cartilage was determined by real-time RT-PCR. In normal samples, HDAC3 was the most abundantly expressed HDAC (data not shown). HDAC7 had significantly higher expression in OA than in normal cartilage (Fig. 2a). Cartilage was obtained from 6 normal donors (mean age 30.8 years; range 19–49 years; Mankin score 0–2 points) and 10 OA donors (mean age 71.6 years; range 44–93 years old; Mankin score 5–10 points) (Fig. 2a). The results are expressed as mean ± SD. $^{*}P < 0.05$. **b–g** HDAC7 localization was examined in tissue from 4 normal donors (age range 19–48 years) and 4 OA donors (age range 48–93 years). HDAC7-positive cells were more frequent in OA cartilage than in normal cartilage. The immunoreactive product is *dark red*. ×10 (**b**, **c**, **e**, **f**). **h** The number of HDAC7-positive cells was counted in the superficial, middle, and deep zones of sections from normal ($n = 4$) and OA ($n = 4$) cartilage with specific antibodies. The OA middle and deep zones had significantly more HDAC7-positive cells than did normal middle and deep zones, respectively. The results are expressed as mean ± SD. $^{*}P < 0.05$, $^{**}P < 0.01$

normal chondrocytes, we used SW1353 human chondrosarcoma cells for this assay (data not shown).

Quantitative polymerase chain reaction

Total RNA was isolated from cartilage tissues or monolayer chondrocyte cultures using Trizol (Invitrogen Inc., Carlsbad, CA, USA). Complementary DNA was produced using Ready-To-Go You Prime First Strand Beads (GE Health Inc., USA) with 2 μg total RNA and oligo (dT) primers. Messenger RNA expression of HDAC1–11 and MMP-13 was detected by real-time RT-PCR with TaqMan Gene Expression Assay probe (Applied Biosystems Inc.) using an iCycler (Bio-Rad Laboratories Inc., Hercules, CA, USA) as follows: 10 min at 95°C for initial denaturation, followed by 45 cycles at 95°C (15 s) and 60°C (1 min). The expression levels of HDACs and MMP-13 were defined from the threshold cycle (Ct) and relative values were calculated by the $2^{-\Delta\Delta Ct}$ method after normalizing expression to GAPDH.

Histology and immunohistochemistry

Cartilage tissues were fixed with 4% paraformaldehyde and stained with Safranin O. HDAC7 antibodies were purchased from Santa Cruz Biotechnologies (catalog no. sc-11421, Santa Cruz, CA, USA). Paraffin-fixed samples were first deparaffinized in xylene substitute Pro-Par Clearant (Anatech Ltd, Battle Creek, MI, USA) and ethanol before rehydration in water. Following a wash with phosphate-buffered saline (PBS), sections were blocked with 0.1% Tween 20 with 3% normal goat serum for 30 min at room temperature. HDAC7 antibodies (1:50 dilution; 4 μg/mL) and normal rabbit immunoglobulin G (IgG, 4 μg/mL) as a negative control were applied and incubated overnight at 4°C. After washing with PBS, sections were incubated with biotinylated goat anti-rabbit secondary antibody for 30 min (1:200; Vector Laboratories Inc., Burlingame, CA, USA) and then incubated with Vectastain ABC-AP kit (AK-5000; Vector Laboratories Inc., Burlingame, CA, USA) for 30 min at room temperature. Finally, sections

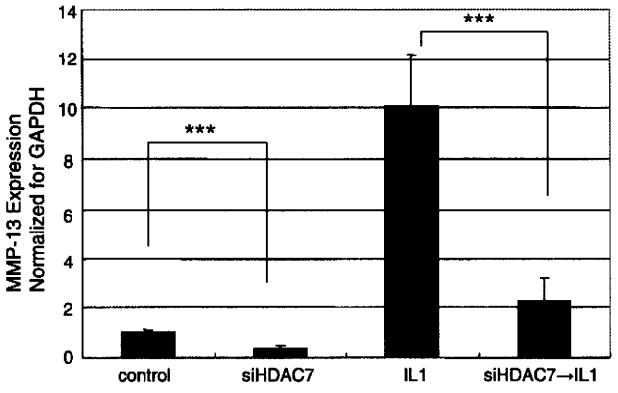

Fig. 3 Knockdown of HDAC7 by siRNA in SW1353 human chondrosarcoma cells. Real-time PCR results of MMP-13 expression in HDAC7 knocked down cells with and without the additional 5 h of culturing in IL-1 (5 ng/mL). Knockdown of HDAC7 decreased both natural and IL-1-induced MMP-13 expression. Data are presented as mean ± SD ($n = 2$, in duplicate). ***$P < 0.001$

were stained with an alkaline phosphatase substrate kit (Vector Laboratories Inc., Burlingame, CA, USA).

Quantification and localization of signals throughout cartilage

To systematically assess HDAC7 localization throughout each cartilage zone, we counted positive and negative cells in a 50 × 50 μm^2 grid (using a 40× field objective) starting from the cartilage surface to the deep zone (DZ). This procedure was repeated a minimum of 5 times for each section. We based our identification of each zone on previously reported characteristics that comprise cell shape, morphology, orientation, and pericellular matrix (PM) deposition [27]. Thus, superficial zone (SZ) cells were characterized by their elongated shape, their parallel orientation relative to the surface, and their lack of extensive PM. These cells predominate within the first 50 μm. The middle zone (MZ) was distinguishable by the presence of rounded cells without an organized orientation relative to the surface, an extracellular matrix (ECM) rich in proteoglycans, and evidence of PM. Conversely, DZ cells were recognized by extensive PM deposition and an organization of 3 or more cells in chondron groups arranged in columns. The depth of each zone was recorded for each section for comparative analysis on the frequency of positive signals in each zone. The frequency of positive cells was expressed as a percentage relative to the total number of cells counted in each zone.

Statistical analysis

Statistically significant differences between 2 groups were determined with t tests. Results are presented as mean ± standard deviation (SD). P values of less than 0.05 were considered statistically significant.

Results

Histone deacetylase inhibitor TSA modulates MMP-13 gene expression

To examine the potential role of HDACs on MMP13 expression, chondrocytes were treated with TSA, a HDAC inhibitor. We used normal chondrocytes ($n = 6$) to exclude effect of OA changes on chondrocytes. When treating human knee chondrocytes with TSA only, natural MMP-13 expression was suppressed to a small degree ($P = 0.120$) and with IL-1 induction of MMP-13 the suppression was greater ($P = 0.067$), but none of the results were statistically significant (Fig. 1). Even though not significant, these results provide a clue and increase our curiosity to which HDAC is affecting the MMP-13 expression.

HDAC7 expression is elevated in OA cartilage

All the knee cartilage samples obtained for this study were examined for HDAC1–11 messenger RNA (mRNA) expressions in human by real-time PCR. Expression of HDAC7 was significantly higher in OA than in normal cartilage (Fig. 2a). On the other hand, HDAC4 and HDAC10 were relatively lower in OA cartilage, although the changes were not statistically significant.

Normal and OA samples stained with Safranin O (Fig. 2b, e) displayed different localization of HDAC7-positive cells. In normal cartilage, we detected positive cells in the MZ (Fig. 2c), whereas in OA cartilage we detected many positive cells, especially in chondrocyte clusters (Fig. 2f, g). Representative examples were a normal 19-year-old female (Mankin score 1) and a 57-year-old male with OA (Mankin score 9). Figure 2h presents the quantitative analysis of zonal distribution of HDAC7-expressing cells in 4 normal (range 19–48 years old) and OA (range 48–93 years old) donors. Complete erosion of the SZ was observed in OA cartilage. Moreover, significantly more positive cells were observed in middle and DZs in OA cartilage, compared with in normal middle and DZs, respectively.

Knockdown of HDAC7 significantly decreases MMP-13 expression

To investigate the correlation between HDAC7 and MMP-13, HDAC7 was knocked down by siRNA in SW1353 human chondrosarcoma cells and mRNA expression of MMP-13 was measured by real-time RT-PCR. HDAC7

knockdown cells were further stimulated with IL-1, and MMP-13 expression was measured again. Knocking down HDAC7 in SW1353 cells decreased both natural and IL-1-induced MMP-13 expression significantly (Fig. 3), indicating functional interaction between HDAC7 and MMP-13.

Discussion

Onset and progression of OA is associated with changes in chondrocyte gene expression. HDACs balance histone acetyltransferases (HATs) and regulate gene transcription epigenetically, and thereby control the acetylation status of histone proteins and nonhistone substrates. In general, acetylation of histones loosens nucleosomal structures, which promotes gene transcription. In contrast, deacetylation of histones stabilizes nucleosomal structures and represses gene transcription [28, 29]. However, emerging evidence indicates that gene regulation by acetylation/deacetylation is more dynamic and complex, and that HATs also can act as repressors and HDACs as transcription activators. Indeed, global analysis of gene expression has shown that inhibition of HDAC activity results in both induction and repression of gene expression [30–35]. Recent studies demonstrated that HDAC inhibitors have therapeutic effects in cancer and inflammatory diseases [14–23]. Young et al. [22] revealed that HDAC inhibitors modulate MMP gene expression in chondrocytes and block cartilage resorption. Although we could not find a statistically significant difference, there is a tendency for MMP13 to be reduced by TSA treatment. As TSA inhibits multiple HDACs, it may be difficult to see direct effect of specific HDAC inhibition by TSA treatment. In this regard, our data showing that specific reduction of HDAC7 by siRNA inhibited MMP-13 expression (Fig. 3) support the idea that HDAC7 promotes MMP-13 in OA pathogenesis.

Matrix metalloproteinases are a family of enzymes that collectively degrade components of the ECM. They are important in normal physiological processes such as development and wound healing, where they appear in a low concentration. In contrast, aberrant MMP expression occurs in several disease states, including atherosclerosis, tumor invasion, and arthritic diseases [36, 37]. MMPs mediate irreversible matrix degradation and subsequent joint destruction in RA and OA. MMP-13 is expressed by chondrocytes and is critical for collagen degradation as it hydrolyzes type II collagen more efficiently than do other collagenases [38]. Therefore, we wanted to see whether a specific HDAC is responsible for IL-1-induced MMP-13 expression and thus contributes to cartilage degradation in OA.

In the present study, we observed significant upregulation of HDAC7 in OA cartilage by real-time RT-PCR and immunohistochemistry (Fig. 2a). HDAC7 is a member of the class II HDACs, which comprises HDAC4, 5, 6, 7, 9, and 10, all of which display cell-type-restricted patterns of expression and contain a highly conserved C-terminal deacetylase catalytic domain. Class II HDACs also contain an N-terminal extension that links them to specific transcription factors and confers responsiveness to a variety of signal transduction pathways serving as a link between the genome and the extracellular environment [39]. Disruption of the HDAC7 gene in mice results in embryonic lethality due to a failure of endothelial cell–cell adhesion and consequent dilatation and rupture of blood vessels. HDAC7 represses MMP-10 gene transcription by associating with myocyte enhancer factor-2 (MEF2), a direct activator of MMP-10 transcription and an essential regulator of angiogenesis [40].

Recently, Jensen et al. [41] demonstrated that HDAC7 associates with Runx2 and represses its activity during osteoblast maturation. Runx2 is required for MMP-13 promoter activity induced by IL-1 [42]. Increased expression of Runx2 in OA cartilage may contribute to increased expression of MMP-13 [43]. Kawaguchi [44] proposed that endochondral ossification signals, in which Runx2 plays a central role, may be important for OA progression [45]. The expression pattern of HDAC7 is different between normal and OA cartilage and the localization of HDAC7 in OA is similar to Runc2 expression in OA [43], suggesting the potential link between Runx2 and HDAC7 in OA pathogenesis. It will be interesting to test whether HDAC7 and Runx2 may cooperatively regulate MMP13 in chondrocytes.

The human genome contains only 18 HDAC genes, but more than 1,800 genes are predicted to encode transcription factors [46]. Given the number of other mechanisms for regulation of MMP-13 expression [47–53], it is important to identify the precise mechanism for how HDAC7 may regulate MMP-13 via specific transcription factors in OA chondrocytes. On the other hand, it is likely that HDAC7 regulates many other OA-related genes. Based on our current study showing the link between HDAC7 and MMP-13 in OA chondrocytes, it is important to examine other HDAC7 targets in OA pathogenesis and test whether HDAC7 could be a therapeutic target by in vivo study.

Conclusions

Our findings support the idea that HDAC7 expression is elevated in human OA cartilage and promotes IL-1 induction of MMP13, contributing to cartilage degradation. Many enigmatic interactions remain unclear, and further

studies are needed to elucidate the mechanism of cartilage degradation by MMP-13 in OA.

Acknowledgments This study was supported by NIH grants AR056120, AR050631, AG007996, and AG033409.

Conflict of interest statement None.

References

1. Pelletier JP, Martel-Pelletier J, Abramson SB. Osteoarthritis, an inflammatory disease: potential implication for the selection of new therapeutic targets. Arthritis Rheum. 2001;44(6):1237–47.
2. Goldring MB. The role of the chondrocyte in osteoarthritis. Arthritis Rheum. 2000;43(9):1916–26.
3. Goldring MB, Berenbaum F. The regulation of chondrocyte function by proinflammatory mediators prostaglandins and nitric oxide. Clin Orthop Relat Res. 2004;427(suppl):S37–46.
4. Bau B, Gebhard PM, Haag J, Knorr T, Bartnik E, Aigner T. Relative messenger RNA expression profiling of collagenases and aggrecanases in human articular chondrocytes in vivo and in vitro. Arthritis Rheum. 2002;46(10):2648–57.
5. Billinghurst RC, Dahlberg L, Ionescu M, Reiner A, Bourne R, Rorabeck C, et al. Enhanced cleavage of type II collagen by collagenases in osteoarthritic articular cartilage. J Clin Invest. 1997;99(7):1534–45.
6. Neuhold LA, Killar L, Zhao W, Sung ML, Warner L, Kulik J, et al. Postnatal expression in hyaline cartilage of constitutively active human collagenase-3 (MMP-13) induces osteoarthritis in mice. J Clin Invest. 2001;107(1):35–44.
7. Gregoretti IV, Lee YM, Goodson HV. Molecular evolution of the histone deacetylase family: functional implications of phylogenetic analysis. J Mol Biol. 2004;338(1):17–31.
8. de Ruijter AJ, van Gennip AH, Caron HN, Kemp S, van Kuilenburg AB. Histone deacetylases (HDACs): characterization of the classical HDAC family. Biochem J. 2003;370(Pt 3):737–49.
9. Bernstein BE, Tong JK, Schreiber SL. Genomewide studies of histone deacetylase function in yeast. Proc Natl Acad Sci USA. 2000;97(25):13708–13.
10. Mulholland NM, Soeth E, Smith CL. Inhibition of MMTV transcription by HDAC inhibitors occurs independent of changes in chromatin remodeling and increased histone acetylation. Oncogene. 2003;22(31):4807–18.
11. Nair AR, Boersma LJ, Schiltz L, Chaudhry MA, Muschel RJ. Paradoxical effects of trichostatin A: inhibition of NF-Y-associated histone acetyltransferase activity, phosphorylation of hGCN5 and downregulation of cyclin A and B1 mRNA. Cancer Lett. 2001;166(1):55–64.
12. Pujuguet P, Radisky D, Levy D, Lacza C, Bissell MJ. Trichostatin A inhibits beta-casein expression in mammary epithelial cells. J Cell Biochem. 2001;83(4):660–70.
13. Saunders N, Dicker A, Popa C, Jones S, Dahler A. Histone deacetylase inhibitors as potential anti-skin cancer agents. Cancer Res. 1999;59(2):399–404.
14. Lin HY, Chen CS, Lin SP, Weng JR. Targeting histone deacetylase in cancer therapy. Med Res Rev. 2006;26(4):397–413.
15. Villar-Garea A, Esteller M. Histone deacetylase inhibitors: understanding a new wave of anticancer agents. Int J Cancer. 2004;112(2):171–8.
16. Johnstone RW. Histone-deacetylase inhibitors: novel drugs for the treatment of cancer. Nat Rev Drug Discov. 2002;1(4):287–99.
17. Kortenhorst MS, Carducci MA, Shabbeer S. Acetylation and histone deacetylase inhibitors in cancer. Cell Oncol. 2006;28(5–6):191–222.
18. Blanchard F, Chipoy C. Histone deacetylase inhibitors: new drugs for the treatment of inflammatory diseases? Drug Discov Today. 2005;10(3):197–204.
19. Lin HS, Hu CY, Chan HY, Liew YY, Huang HP, Lepescheux L, et al. Anti-rheumatic activities of histone deacetylase (HDAC) inhibitors in vivo in collagen-induced arthritis in rodents. Br J Pharmacol. 2007;150(7):862–72.
20. Nasu Y, Nishida K, Miyazawa S, Komiyama T, Kadota Y, Abe N, et al. Trichostatin A, a histone deacetylase inhibitor, suppresses synovial inflammation and subsequent cartilage destruction in a collagen antibody-induced arthritis mouse model. Osteoarthr Cartil. 2008;16(6):723–32.
21. Nishida K, Komiyama T, Miyazawa S, Shen ZN, Furumatsu T, Doi H, et al. Histone deacetylase inhibitor suppression of autoantibody-mediated arthritis in mice via regulation of p16INK4a and p21(WAF1/Cip1) expression. Arthritis Rheum. 2004;50(10):3365–76.
22. Young DA, Lakey RL, Pennington CJ, Jones D, Kevorkian L, Edwards DR, et al. Histone deacetylase inhibitors modulate metalloproteinase gene expression in chondrocytes and block cartilage resorption. Arthritis Res Ther. 2005;7(3):R503–12.
23. Chabane N, Zayed N, Afif H, Mfuna-Endam L, Benderdour M, Boileau C, et al. Histone deacetylase inhibitors suppress interleukin-1beta-induced nitric oxide and prostaglandin E2 production in human chondrocytes. Osteoarthr Cartil. 2008;16(10):1267–74.
24. Thomas CM, Fuller CJ, Whittles CE, Sharif M. Chondrocyte death by apoptosis is associated with cartilage matrix degradation. Osteoarthr Cartil. 2007;15(1):27–34.
25. Blanco FJ, Ochs RL, Schwarz H, Lotz M. Chondrocyte apoptosis induced by nitric oxide. Am J Pathol. 1995;146(1):75–85.
26. Otsuki S, Taniguchi N, Grogan SP, D'Lima D, Kinoshita M, Lotz M. Expression of novel extracellular sulfatases Sulf-1 and Sulf-2 in normal and osteoarthritic articular cartilage. Arthritis Res Ther. 2008;10(3):R61.
27. Guilak F, Alexopoulos LG, Upton ML, Youn I, Choi JB, Cao L, et al. The pericellular matrix as a transducer of biomechanical and biochemical signals in articular cartilage. Ann N Y Acad Sci. 2006;1068:498–512.
28. Jenuwein T, Allis CD. Translating the histone code. Science. 2001;293(5532):1074–80.
29. Urnov FD. Chromatin remodeling as a guide to transcriptional regulatory networks in mammals. J Cell Biochem. 2003;88(4):684–94.
30. Kruh J. Effects of sodium butyrate, a new pharmacological agent, on cells in culture. Mol Cell Biochem. 1982;42(2):65–82.
31. Chang S, Pikaard CS. Transcript profiling in Arabidopsis reveals complex responses to global inhibition of DNA methylation and histone deacetylation. J Biol Chem. 2005;280(1):796–804.
32. Reid G, Metivier R, Lin CY, Denger S, Ibberson D, Ivacevic T, et al. Multiple mechanisms induce transcriptional silencing of a subset of genes, including oestrogen receptor alpha, in response to deacetylase inhibition by valproic acid and trichostatin A. Oncogene. 2005;24(31):4894–907.
33. Nawaz Z, Baniahmad C, Burris TP, Stillman DJ, O'Malley BW, Tsai MJ. The yeast SIN3 gene product negatively regulates the activity of the human progesterone receptor and positively regulates the activities of GAL4 and the HAP1 activator. Mol Gen Genet. 1994;245(6):724–33.
34. Mariadason JM, Corner GA, Augenlicht LH. Genetic reprogramming in pathways of colonic cell maturation induced by short chain fatty acids: comparison with trichostatin A, sulindac,

and curcumin and implications for chemoprevention of colon cancer. Cancer Res. 2000;60(16):4561–72.
35. Chambers AE, Banerjee S, Chaplin T, Dunne J, Debernardi S, Joel SP, et al. Histone acetylation-mediated regulation of genes in leukaemic cells. Eur J Cancer. 2003;39(8):1165–75.
36. Libby P, Aikawa M. New insights into plaque stabilisation by lipid lowering. Drugs. 1998;56(suppl 1):9–13. (discussion 33).
37. McCawley LJ, Matrisian LM. Matrix metalloproteinases: multifunctional contributors to tumor progression. Mol Med Today. 2000;6(4):149–56.
38. Mitchell PG, Magna HA, Reeves LM, Lopresti-Morrow LL, Yocum SA, Rosner PJ, et al. Cloning, expression, and type II collagenolytic activity of matrix metalloproteinase-13 from human osteoarthritic cartilage. J Clin Invest. 1996;97(3):761–8.
39. Verdin E, Dequiedt F, Kasler HG. Class II histone deacetylases: versatile regulators. Trends Genet. 2003;19(5):286–93.
40. Chang S, Young BD, Li S, Qi X, Richardson JA, Olson EN. Histone deacetylase 7 maintains vascular integrity by repressing matrix metalloproteinase 10. Cell. 2006;126(2):321–34.
41. Jensen ED, Schroeder TM, Bailey J, Gopalakrishnan R, Westendorf JJ. Histone deacetylase 7 associates with Runx2 and represses its activity during osteoblast maturation in a deacetylation-independent manner. J Bone Miner Res. 2008;23(3):361–72.
42. Mengshol JA, Vincenti MP, Brinckerhoff CE. IL-1 induces collagenase-3 (MMP-13) promoter activity in stably transfected chondrocytic cells: requirement for Runx-2 and activation by p38 MAPK and JNK pathways. Nucleic Acids Res. 2001;29(21):4361–72.
43. Wang X, Manner PA, Horner A, Shum L, Tuan RS, Nuckolls GH. Regulation of MMP-13 expression by RUNX2 and FGF2 in osteoarthritic cartilage. Osteoarthr Cartil. 2004;12(12):963–73.
44. Kawaguchi H. Endochondral ossification signals in cartilage degradation during osteoarthritis progression in experimental mouse models. Mol Cells. 2008;25(1):1–6.
45. Kamekura S, Kawasaki Y, Hoshi K, Shimoaka T, Chikuda H, Maruyama Z, et al. Contribution of runt-related transcription factor 2 to the pathogenesis of osteoarthritis in mice after induction of knee joint instability. Arthritis Rheum. 2006;54(8):2462–70.
46. Venter JC, Adams MD, Myers EW, Li PW, Mural RJ, Sutton GG, et al. The sequence of the human genome. Science. 2001;291(5507):1304–51.
47. Iliopoulos D, Malizos KN, Tsezou A. Epigenetic regulation of leptin affects MMP-13 expression in osteoarthritic chondrocytes: possible molecular target for osteoarthritis therapeutic intervention. Ann Rheum Dis. 2007;66(12):1616–21.
48. Yun K, Im SH. Transcriptional regulation of MMP13 by Lef1 in chondrocytes. Biochem Biophys Res Commun. 2007;364(4):b1009–14.
49. Mengshol JA, Vincenti MP, Coon CI, Barchowsky A, Brinckerhoff CE. Interleukin-1 induction of collagenase 3 (matrix metalloproteinase 13) gene expression in chondrocytes requires p38, c-Jun N-terminal kinase, and nuclear factor kappaB: differential regulation of collagenase 1 and collagenase 3. Arthritis Rheum. 2000;43(4):801–11.
50. Brenner DA, O'Hara M, Angel P, Chojkier M, Karin M. Prolonged activation of jun and collagenase genes by tumour necrosis factor-alpha. Nature. 1989;337(6208):661–3.
51. Conca W, Kaplan PB, Krane SM. Increases in levels of procollagenase messenger RNA in cultured fibroblasts induced by human recombinant interleukin 1 beta or serum follow c-jun expression and are dependent on new protein synthesis. J Clin Invest. 1989;83(5):1753–7.
52. Borden P, Solymar D, Sucharczuk A, Lindman B, Cannon P, Heller RA. Cytokine control of interstitial collagenase and collagenase-3 gene expression in human chondrocytes. J Biol Chem. 1996;271(38):23577–81.
53. Baker AH, Edwards DR, Murphy G. Metalloproteinase inhibitors: biological actions and therapeutic opportunities. J Cell Sci. 2002;115(Pt 19):3719–27.

特集
変形性膝関節症の治療戦略

【診断】

変形性膝関節症に対するMRI診断の位置づけ

MRI examination for osteoarthritic knee : the status quo

佐粧孝久

T. Sasho：千葉大学大学院医学研究院整形外科

Key words

●変形性膝関節症(osteoarthritis of the knee)
●MRI (magnetic resonance imaging)
●WORMS (Whole-Organ magnetic resonance imaging score)
●BLOKS (Boston leeds osteoarthritis knee score)
●KOOS (knee osteoarthritis scoring system)
●不整度計測(irregularity index)

はじめに

変形性膝関節症のX線検査

変形性膝関節症(膝OA)の画像診断ではX線検査が必須の検査となっている。X線検査では骨棘，関節裂隙の狭小化，骨硬化像，骨嚢包などの有無や程度の評価と下肢アライメントの評価が可能である。繁用されているX線分類であるKellgren-Lawrence分類(K-L分類)では骨棘の形成が重要視され[1]，疫学的検討には必須の分類となっている。X線検査は，荷重下に膝の屈曲角度を厳密にコントロールすることで関節裂隙の狭小化を鋭敏に捉えることが可能であり[2]，間接的であるものの，わずかな軟骨の消失をも捉えることができる。そのため薬物療法の効果を調べるバイオモニターとして利用されている。Okaら[3]はX線像を自動的に解析するソフトウエアを開発し，臨床応用への可能性を示唆した。以上のように診断・重症度分類・薬物効果の判定など，目的により撮像法や分類法を選択することでX線検査は有用な検査である。しかしながら，その一方でX線所見と臨床症状にはしばしば解離がみられること，多様な症状を示す患者群をわずかに4段階や5段階に分類することしかできないことなどの問題点があることも事実である。

膝OAのMRI検査

そこで，MRIが膝OAの診断・重症度評価，治療効果の判定などのために用いられるようになってきた。膝OAの病態・臨床症状に関与する組織はX線で捉えられる骨組織の変化に留まらないため，理論的にもMRIがより適していると考えられる。MRIでは軟骨，半月板，大腿骨・脛骨の骨髄の変化，関節水症の程度，滑膜炎の程度を捉えることが可能である。

本稿では，膝OAに対するMRI検査の位置づけについて話を進めていく。そのために大きく2つに分けて論述する。1つ目は膝OAとして症状

0286-5394/10/¥400/論文/JCOPY

を発現する前の軟骨変性を捉えうる検査法であり，2つ目は膝OAを発症した後にその重症度・進行度を判定する検査法である。前者は膝OAの予防や薬物療法の効果を知るために有効であり，後者は罹患膝の状態を評価し適切な治療法を選択するために必要となる検査法であるといえよう。

軟骨の初期変性を捉える撮像法

さまざまな撮像法が考案され試行されているが，代表的な撮像法を4つ取り上げたい。いずれも膝OAの初期変性を捉えるものであり，バイオマーカーとしての応用が期待されている。

three-dimensional spoiled gradient-recalled (3D-SPGR法)

主として水分含量を鋭敏に捉え，軟骨の厚み，ボリュームの評価に適している。三次元撮像のため膝全体の軟骨の評価が可能であり，軟骨とほかの組織のコントラストが良好なため，画像解析ソフトと組み合わせることで膝全体の軟骨だけを抽出して評価することも可能である[4]。代表例を**図1**に示した。

遅延相軟骨造影MRI (delayed gadolinium enhanced magnetic resonance imaging for cartilage；dGEMRIC)

造影剤である$Gd\text{-}DTPA^{2-}$を経静脈的に投与して撮像する。造影剤を投与してから軟骨に$Gd\text{-}DTPA^{2-}$が均一に浸透した後に撮像することから遅延相とよばれる。陰性荷電した$Gd\text{-}DTPA^{2-}$と同様に陰性荷電をもつ軟骨基質の主要な構成成分であるglucosamino-glycan(GAG)が反発し合う性質を応用したものである[5]。すなわちGAG濃度の低い部位では$Gd\text{-}DTPA^{2-}$が高濃度に分布し，GAG濃度の高い部位では$Gd\text{-}DTPA^{2-}$が低濃度に分布することになるのである。臨床的には，前十字靱帯損傷時に大腿骨外側顆の骨挫傷部にみられる軟骨損傷や，半月板損傷または切除後に合併してみられる軟骨変性などの診断が可能であると報告されている[6]。また，軟骨修復術後の経時的な軟骨の質的変化を評価できる方法としても報告されている[7]。本法はGAG濃度を唯一のパラメータとする方法であり，初期OAの軟骨変性を捉える方法として有望である。ただし造影剤を使用せざるをえないのが欠点であり，無症状である膝に対するスクリーニングと

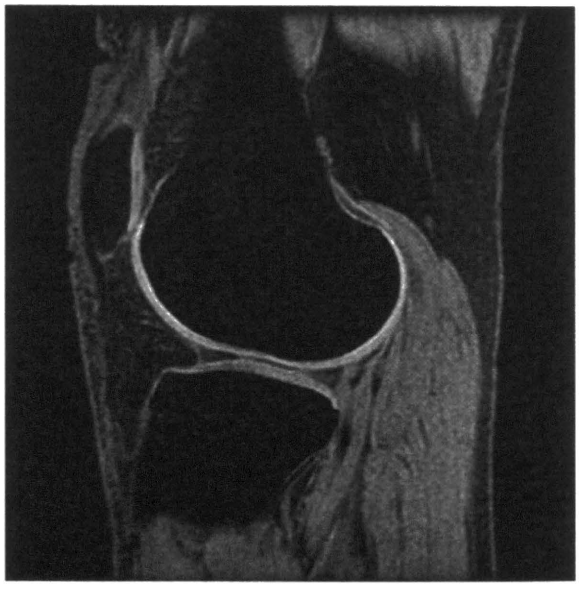

図1 【症例1】3D-SPGR法
50歳代，男性。外側コンパートメントの矢状断像である。膝蓋骨，大腿骨，脛骨の軟骨の厚みが低輝度の領域として明瞭に描出されている。

しては問題がある。また，現在までの報告の多くでは代表的な1スライスしか撮像できていないため，膝全体の評価法としてはさらなる発展が望まれる。代表例を**図2，3**に示した。

T2 mapping

軟骨の構成成分のうち水分含量，コラーゲン配列の2つをパラメータとする。軟骨基質のコラーゲン配列は層ごとに異なるためマッピング上，正常でも均一とはならず，正常軟骨においてもT2は表層で長く，中間層，深層で短くなる。そのため表層にみられるT2の延長を変性と解釈する可能性があること，マジックアングル効果の影響を大きく受けることが問題となる[6]。とくに矢状断像ではアーチファクトを生じやすい。代表例を**図4**に示した。

T1 rho

造影剤を用いなくてもGAGの評価が可能な方法として期待されている。比較的最近になり確立してきた方法であるため，臨床的な応用・知見はほかの方法に比べると少ない。dGEMRICと同様に，主にGAG濃度を反映するものであるが，OAが進行するとコラーゲンの変化も反映

図2 【症例2】dGEMRIC
30歳代，女性。膝蓋骨亜脱臼のある膝関節の横断像である。膝蓋骨の軟骨をカラーマッピングにて表示している。
a：ヒアルロン酸製剤投与前。
b：ヒアルロン酸製剤投与後。表層軟骨のGAG濃度が改善したことが示唆される。

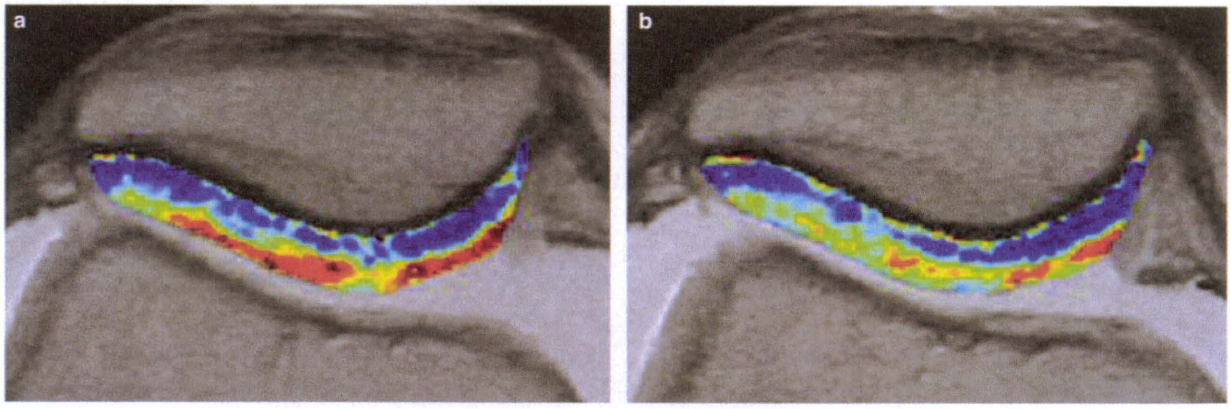

図3 【症例3】dGEMRIC
30歳代，男性。前十字靱帯断裂時にみられた大腿骨顆部骨挫傷に相当する部位に赤色で示される軟骨の変性が認められた(矢印)。

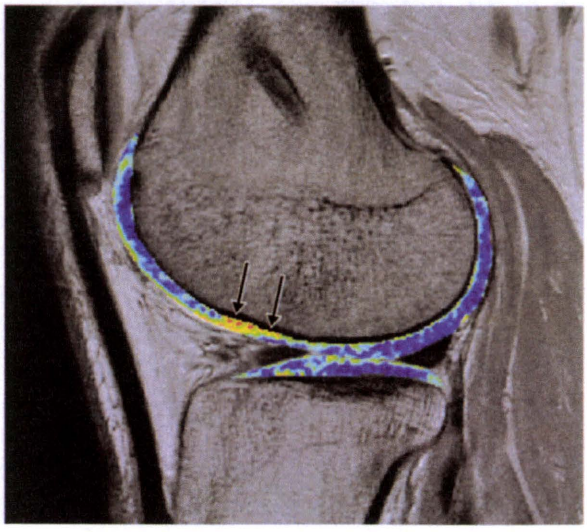

すると考えられている[8]。今後の発展が期待されている撮像法である。

各々の撮像法は個々にも軟骨の初期変性を捉えるものとして期待されているが，組み合わせることでより膝OAの病態を詳細に理解することを助けるものとなりうる。しかしながら，撮像時間が長くなること，できるだけ高磁場の撮像装置が望ましいことなどから，一般的に普及するには至っていない。

重症度・進行度の評価法

本稿では4つの方法を取り上げたい。前半の3つの方法は膝関節の状態を半定量的に示すものである。Whole-Organ magnetic resonance imaging score (WORMS)，Boston leeds osteoarthritis knee score (BLOKS)，knee osteoarthritis scoring system (KOOS) の3つの方法である。どの方法も基本的には関節を区域に分け，各々の区域内での関節を構成する要素をグレーディングし点数化するものである。各々の方法で区域分けの方法や対象とする組織，グレーディングの数などに違いがある。現時点ではWORMSが最も広く使用されている。4番目に取り上げる不整度評価法は著者らが提唱している方法であり，大腿骨顆部の輪郭の不整度のみを数値化するものである。

図4 【症例4】T2 mapping

30歳代，女性。膝関節痛のため精査を行ったT2 mapping像。カラーバーの赤色はT2の長い変性部位を，青色はT2の短い健常部位を示す。単純X線や通常のMRIでは明らかな異常所見を指摘できなかったが，大腿骨内側顆および脛骨内側顆に軟骨のT2延長が認められ（矢頭印），同部にコラーゲン配列の不整化などを伴う軟骨変性の存在が示唆された。

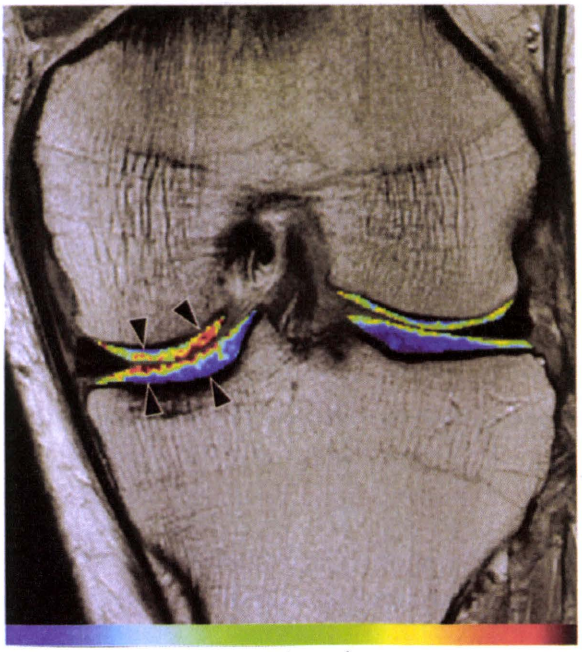

（文献[6]より）

WORMS

2004年にPeterfyら[9]により報告された方法である。膝関節を15の区域に分け**(図5)**それぞれの区域の軟骨，骨髄の輝度変化，bone cyst，bone attrition，骨棘，半月板，靱帯などの評価を行い，MRI所見を点数化する方法であり，膝関節の全体的な評価だけではなく内外側コンパートメント，膝蓋大腿コンパートメントといったコンパートメントごとの評価も可能という特徴がある。WORMS点数はMRI上まったく所見がなければ0点であり，最高点は332点である。

BLOKS

2008年にHunterら[10]により報告された。膝関節を9つの区域に分け評価対象となる組織に点数をつけていくものである。WORMSと異なるのはbone attritionを評価に含まないことである。

KOOS

2005年にKomaatら[11]により報告された。膝関節を9つに分け評価するが，BLOKSとは異なる分け方を採用している。WORMSと比較し靱帯，遊離体を評価に含まないという特徴がある。

不整度評価法

膝OAが進行すると明らかになってくる，大腿骨顆部の輪郭の不整の程度を数値化する方法であり，JOAスコア，Japan knee osteoarthritis measure (JKOM) と相関することが示されている[12)~14)]。また，臨床応用として治療法の選択する際の指標となる可能性を報告している[15)]。

WORMSとの比較でもほぼ同等に使用できることもわかっている[16]。不整度とWORMSにより評価した代表的な2例を**図6**に示した。

重症度・進行度評価法の現状

膝OAの重症度・進行度評価法は，

①進行度の評価

②進行度の評価に基づく治療体系の作成

③治療効果の判定

④経時的なモニタリングなど

に応用可能であり，高齢社会において必要性が高くなってくるものである。しかしながら，「1.わが国の患者群に適応するためにどの方法がよいのか」，「2.なんらかの修正が必要となるのか」，「3.目的に応じて使用すべき方法が異なるのか」，など解決すべき問題がある。

まとめ

膝OAは高齢者のQOLを著しく低下させる大きな問題である。そのため膝OAの早期発見や予防法が大切な課題となってきている。この目的のためにはスクリーニング検査が必要となり，MRIが最も有力な手段と考えられる。しかしながら撮像時間が長いことやコストがかさむことなどの理由もあり，一般化するには至っていない。また，重症度を評価する方法が考案されてきており，さらなる発展と臨床への応用が期待されている。

図5 WORMSで用いられている膝関節の区域分け

WORMSでは膝関節の膝伸展位MRIを15の区域に分ける。S領域以外の14の区域について軟骨を8段階，骨髄病変を4段階，骨嚢包を4段階，bone attritionを4段階，骨棘を8段階のグレードで評価し評点を与える。S領域については骨髄病変と骨嚢包のみ評価する。その他に半月板，靱帯，滑膜炎の程度を評価し点数を合計することでその膝の重症度が定まる。

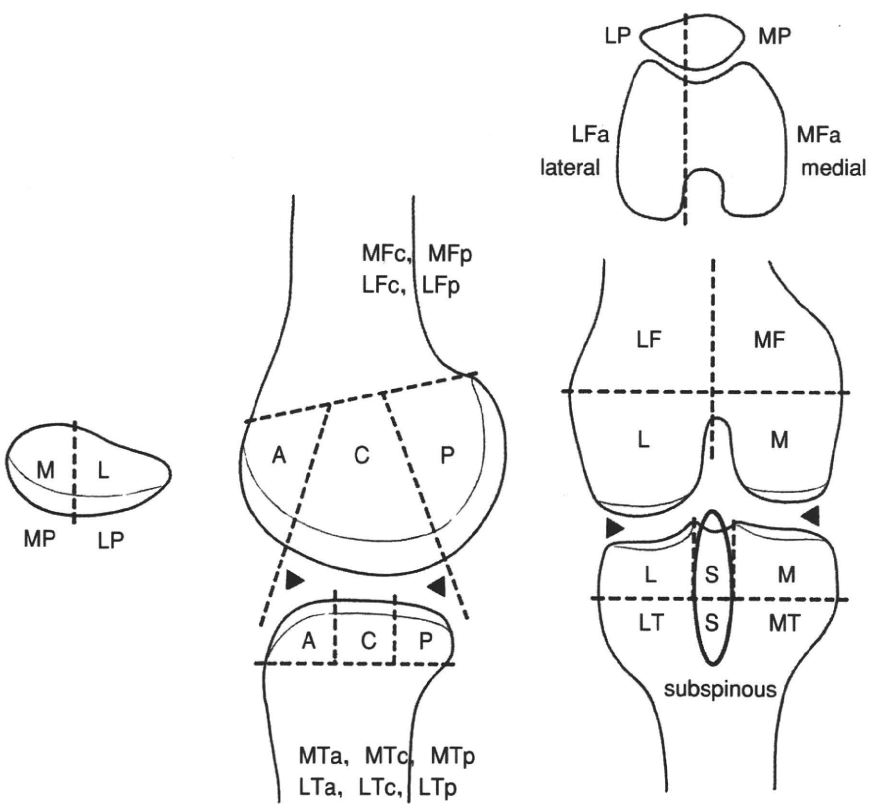

（文献[9]より）

図6 X線所見とWORMSおよび不整度

ともに60歳代後半，女性の膝関節の画像所見である。

【症例5】

a：単純X線正面像。

b：内側コンパートメントのプロトン密度強調像の矢状断像。

c：**b**を白黒画像に変換したもの。K-L分類ではグレードⅣである。

【症例6】

d：単純X線正面像。

e：内側コンパートメントのプロトン密度強調像の矢状断像。

f：**e**を白黒画像に変換したもの。K-L分類ではグレードⅢである。

両者のWORMSは75，78とあまり差がなく，**c**，**f**内の矢印で示した大腿骨内側顆の不整度を計測したところ，2.40および2.48と不整度の差も少なかった。X線とMRIでは評価が異なることを示す代表例である。

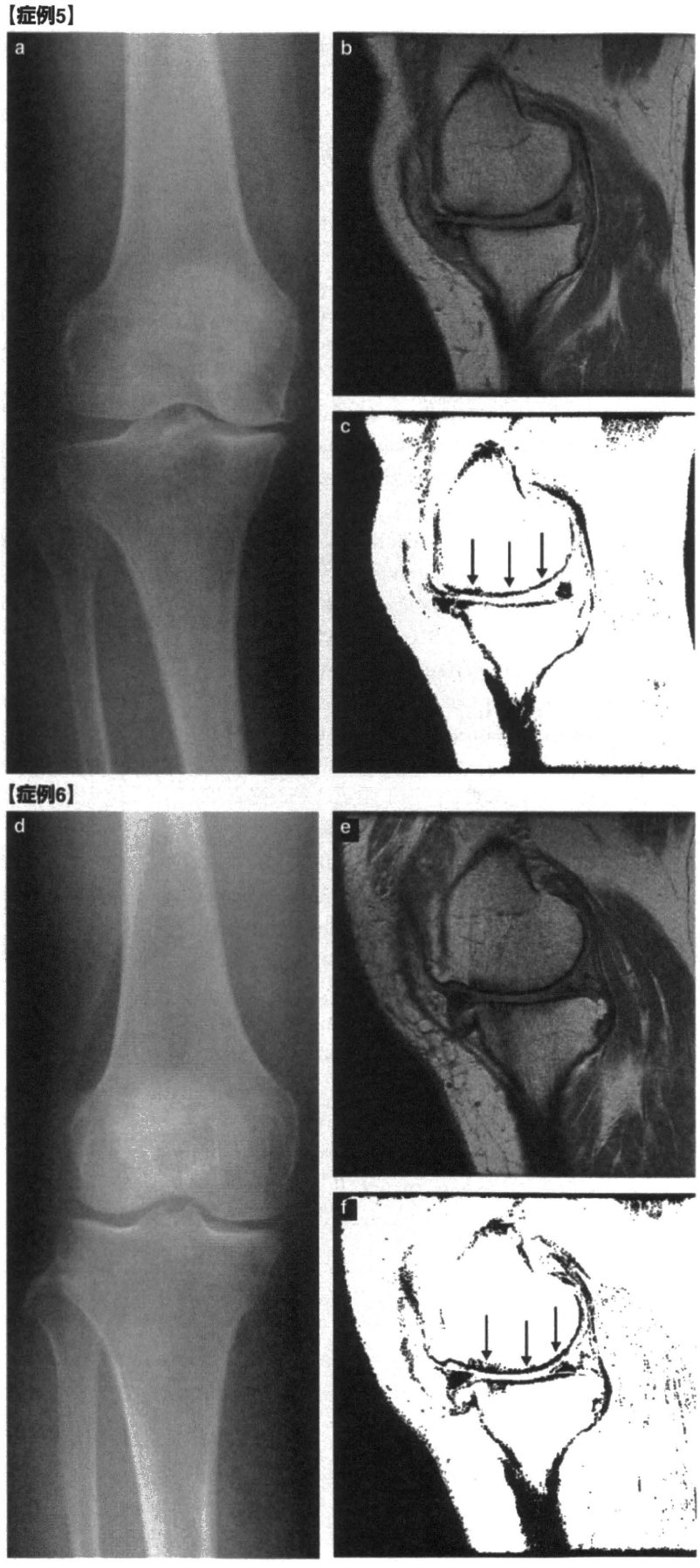

文献

1)Kellgren J, Lawrence J：Radiological assessment of osteo-arthrosis. Ann Rheum Dis, 16：494-502, 1957.

2)Radiography Working Group of the OARSI-OMERACT Imaging Workshop, Le Graverand MP, Mazzuca S, Lassere M, et al：Assessment of the radioanatomic positioning of the osteoarthritic knee in serial radiographs：comparison of three acquisition techniques. Osteoarthritis Cartilage, 14(Suppl A)：A37-43, 2006.

3)Oka H, Muraki S, Akune T, et al：Fully automatic quantification of knee osteoarthritis severity on plain radiographs. Osteoarthritis Cartilage, 16(11)：1300-1306, 2008.

4)Brem MH, Pauser J, Yoshioka H, et al：Longitudinal *in vivo* reproducibility of cartilage volume and surface in osteoarthritis of the knee. Skeletal Radiol, 36(4)：315-320, 2007.

5)Bashir A, Gray ML, Hartke J, et al：Nondestructive imaging of human cartilage glycosaminoglycan concentration by MRI. Magn Reson Med, 41：857-865, 1999.

6)渡辺淳也，大久保敏之，山下剛司ほか：遅延相造影MRIおよびT2マッピングによる変性軟骨の質的評価. 関節外科, 27：229-234, 2008.

7)Watanabe A, Wada Y, Obata T, et al：Time course evaluation of reparative cartilage with MR imaging after autologous chondrocyte implantation. Cell Transplantation, 14：695-700, 2005.

8)Ragatte RR, akella SVS, Wheaton AJ, et al：3D-T1p-relaxation mapping of articular cartilage. Acad Radiol, 11：741-749, 2004.

9)Peterfy CG, Guermazi A, Zaim S：Whole-Organ magnetic resonance imaging score(WORMS) of the knee in osteoarthritis. Osteoarthritis Cartilage, 12：177-190, 2004.

10)Hunter DJ, Lo GH, Gale D, et al：The reliability of a new scoring system for knee osteoarthritis MRI and the validity of bone marrow lesion assessment：BLOKS(Boston leeds osteoarthritis knee score). Ann Rheum Dis, 67：206-211, 2008.

11)Komaat PR, Ceulemans RY, Kroon HM, et al：MRI assessment of knee osteoarthritis：Knee osteoarthritis scoring system(KOSS)? inter-observer and intra-observer reproducibility of a compartment-based scoring system. Skeletal Radiol, 34：95-102, 2005.

12)佐粧孝久，中川晃一，鈴木昌彦ほか：MRIを用いた変形性膝関節症の客観的な重症度評価指数の確立. 日整会誌, 81：29-35, 2007.

13)Iwasaki J, Sasho T, Nakagawa K, et al：Irregularity of medial femoral condyle on MR imaging serves as a possible indicator of objective severity of medial-type osteoarthritic knee. Clin Rheumatol, 26(10)：1705-1708, 2007.

14)Ochiai N, Sasho T, Tahara M, et al：Objective assessments of medial osteoarthritic knee severity by MRI：new computer software to evaluate femoral condyle contours. International Orthopaedics, 2009.

15)佐粧孝久，落合信靖，松木　恵ほか：変形性膝関節症に対するMRIを用いた重症度評価法に基づく治療法の選択. 関節外科, 27(10月増刊号)：109-115, 2008.

16)松木　恵，佐粧孝久，中川晃一ほか：MRIによる変形性膝関節症の重症度評価法－大腿骨顆部輪郭の不整度とWORMSの比較－. 膝, 33：33-38, 2008.

International Orthopaedics (SICOT) (2010) 34:811–817
DOI 10.1007/s00264-009-0864-4

ORIGINAL PAPER

Objective assessments of medial osteoarthritic knee severity by MRI: new computer software to evaluate femoral condyle contours

Nobuyasu Ochiai · Takahisa Sasho · Masamichi Tahara · Atsuya Watanabe · Kei Matsuki · Satoshi Yamaguchi · Yoichi Miyake · Toshiya Nakaguchi · Yuichi Wada · Hideshige Moriya

Received: 7 July 2009 / Revised: 30 July 2009 / Accepted: 18 August 2009 / Published online: 8 September 2009

Abstract An irregular contour of the medial femoral condyle (MFC) on magnetic resonance imaging (MRI) appears to indicate the severity of medial-type knee osteoarthritis (OA). The purpose of this study was to establish a system to enable objective assessments of OA knee severity using newly developed software that semi-automatically measures irregularity of the MFC. (1) We evaluated 48 patients aged 50–83 years with 55 knees of medial-type OA. The following scores were recorded: Lysholm score, visual analogue scale (VAS) and the Japanese Knee Osteoarthritis Measure (JKOM). MFC irregularity was automatically calculated by newly programmed computer software. Four parameters for condyle irregularity were calculated: (a) the average thickness of the contour (ATC), (b) the ratio of the upper surface length to the lower surface length of the contour (RUL), (c) average squared thickness of the contour (ASTC) and (d) standard deviation of the contour thickness (SDC). (2) Nine knees that underwent total knee arthroplasty were further analysed histopathologically and compared with irregularity score. Statistically, the RUL and SDC were significantly correlated with the Lysholm score, VAS and JKOM, with good reliability. Histological examinations showed that an irregular contour reflected the density of cystic lesions formed in subchondral bone. An irregularity of MFC on MRI is correlated with OA disease severity clinically and histopathologically. The new computer software is useful to objectively assess OA disease severity.

Nobuyasu Ochiai and Takahisa Sasho contributed equally to this study.

N. Ochiai · T. Sasho (✉) · M. Tahara · K. Matsuki · S. Yamaguchi · H. Moriya
Department of Orthopedic Surgery, Graduate School of Medicine, Chiba University,
1-8-1 Inohana, Chuo-ku,
Chiba 260-8670, Japan
e-mail: sasho@faculty.chiba-u.jp

A. Watanabe · Y. Wada
Department of Orthopaedic Surgery,
Teikyo University Ichihara Hospital,
Chiba, Japan

Y. Miyake · T. Nakaguchi
Research Center for Frontier Medical engineering,
Chiba University,
Chiba, Japan

Introduction

Osteoarthritis (OA) of the knee joint is a common joint pathology. X-ray examination is generally performed to assess the status of the OA knee joint, as it identifies the characteristic features of osteophytes, thickening of subchondral bone, cyst formation, malalignment and reduction of joint space due to cartilage loss. Among the indices to assess severity of OA using X-ray, the Kellgren-Lawrence (K/L) scale [1, 2] is frequently used and believed to be mostly reliable. However, its actual relationship with clinical severity of OA is controversial.

Magnetic resonance imaging (MRI) has also been used to evaluate OA knee joints due to its ability to detect cartilage abnormalities, osteophytes, subarticular cysts, bone attrition, synovitis, meniscal degeneration, bone marrow oedema, joint effusion, intra-articular loose body and periarticular cysts [3]. However, the clinical meanings of these abnormalities are not fully defined. One reason for this might be that the chief complaint of most patients is not

deformity but knee pain, and the pain mechanisms of OA are not fully understood.

Recent evidence suggests that the subchondral bone is important for both pain origination and OA progression [4–6]. On MRI, contours of the femoral condyle or the tibial plateau are often depicted with irregularities, which could correspond to thickening of subchondral bone seen on X-ray [7]. In a pilot study, we reported that irregularities of the femoral condyle on MRI and knee functional scores were inter-related. In that study, calculation of irregularity was done with software that was developed for another purpose [8]. This result prompted us to develop new computer software that exclusively measures the irregularity of the femoral condyle.

Our hypothesis is that an irregular contour of the femoral condyle on MRI could be an indicator of OA disease severity and that measuring the irregularity of the contour should enable us to objectively assess OA severity. The purpose of this study was to develop new computer software that could exclusively measure the irregular contour of the femoral condyle and establish a reliable index that reflected OA severity. The relationship between OA clinical severity and femoral condyle irregularity was examined. Histological examination was performed as well.

Materials and methods

Patients and clinical assessments

Forty-eight consecutive patients with a total of 55 knee joints were recruited for this study. Patients with a history of trauma, previous surgery or inflammatory arthritis were excluded. Patients' mean age was 72.8 (range 50–83) years. None had prior surgical treatment. Informed consent was obtained from all patients after the nature of the examinations had been fully explained. All examinations were performed in accordance with the rules and regulations of the local human research committee. All patients were clinically examined at their first visit. They were scored using the Lysholm score [9], visual analogue scale [(VAS) on a 100-cm scale: 0 = no pain; 100 = most severe pain] and the Japanese Knee Osteoarthritis Measure (JKOM) [10]. Lysholm scores without items for instability were used. The JKOM is a counterpart of the Western Ontario and McMaster Osteoarthritis Index (WOMAC) that was developed for assessing Japanese OA patients by taking the Japanese lifestyle into account. It has proved to be as good as or better than the WOMAC or the Medical Outcomes Study 36-Item Short-Form Health Survey (SF-36) in terms of its reliability and validity [10].

Imaging

All patients underwent MRI of the affected knees within two weeks of their first visit. MRI was performed with a 1.5-T scanner (Signa, GE Medical Systems) equipped with a knee surface coil. The sequence used in this study was sagittal fast spin echo (FSE) proton density (TR 2,000 ms, TE 16 ms, field of view 14–16 cm, matrix 512 × 512, number of excitations = 2, and slice thickness = 4 mm without an interslice gap). Three sagittal slices that represented the centre of the medial femoral condyle (MFC) were selected for analysis by two orthopaedic surgeons who reached a consensus without knowledge of patient age or sex. The lateral femoral condyle (LFC) was assessed as well. X-ray grading employing the K/L scale [1] on weight-bearing radiographs was also recorded.

Software interface

Irregularity of the contour of the femoral condyle was calculated by computer software that was programmed in MATLAB6.5 (Cyber Net Systems, Tokyo). Digital Imaging and Communication in Medicine (DICOM) data can be incorporated directly with this software. The procedures used to measure the irregularity of the contour of the MFC were as follows: (1) Images to be assessed were selected. Images that represented the centre of the medial compartment were selected. Usually, six or seven images were taken for a medial compartment and three slices that represented the centre of the compartment were selected. (2) The image was converted to black and white (Fig. 1b). The threshold between black and white was determined by the histogram of the dots comprising images. With the vertical axis defined as the number of dots and the horizontal axis as the luminescence of dots, the histograms of these images usually consisted of two or three peaks. The threshold was determined manually so as to leave only the first peak. This meant that only very low luminescence dots remained; i.e., only very black dots. (3) The contour of the MFC was extracted (Fig. 1c), after which the upper and the lower surfaces of the extracted contour were automatically traced (Fig. 1d). Using these two lines, four parameters reflecting irregularity were automatically calculated: (a) average thickness of the contour (ATC), (b) ratio of the length of the upper surface to the lower surface length of the contour (RUL), (c) average squared thickness of the contour (ASTC) and (d) standard deviation of contour thickness (SDC). Theoretically, the more obvious the irregularity or thickening becomes, the larger the ATC, RUL, ASTC and SDC values become.

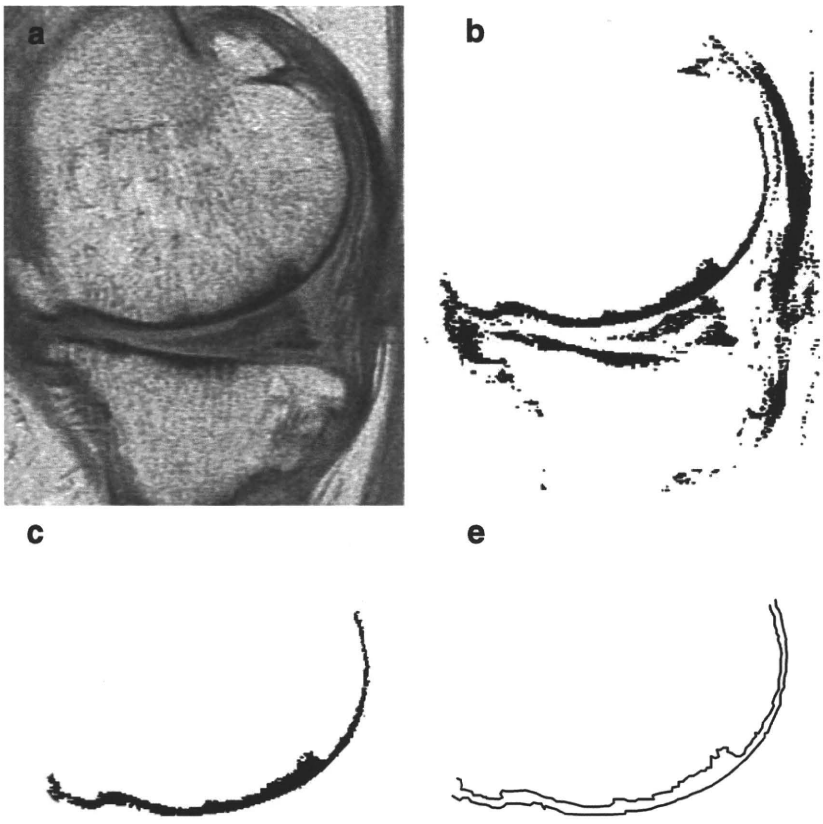

Fig. 1 Procedures to calculate irregularity of the condyle. **a** Image to be assessed is selected on the personal computer (PC). **b** The image is then converted to black and white. **c** Only the condyle contour is extracted. **d** The upper and lower surfaces of the extracted contour are traced, making two lines. Using these two lines, parameters reflecting irregularity are calculated

Interobserver and intraobserver reliabilities

Using ten randomly selected knees of the 55 knees evaluated, intra- and interrater reliabilities, intraclass correlation coefficient (ICC) (1, 1) and ICC (2, 1) were determined.

Specimens and histological evaluation

Nine knees that underwent total knee arthroplasty (TKA) following MRI assessments were used for this study. At the time of TKA, the weight-bearing areas of the MFC and the LFC were obtained. Specimens were immediately fixed in 4% paraformaldehyde in phosphate-buffered saline for 24 h. The MFC and LFC were demineralised in 20% ethylenediaminetetraacetic acid (EDTA) at room temperature for six weeks. They were then embedded in paraffin. Sagittal sections (6 μm) were made and mounted on glass slides. Following staining with Mayer's haematoxylin solution and 1% eosin alcohol solution (H&E staining), the total number of cystic lesions that invaded the subchondral bone plate or calcified zone were counted from three slides that corresponded to weight-bearing areas. Density of cystic lesions was expressed as the number of cystic lesions per 10-mm-length of specimen [11]. Correlation of parameters related to irregularity of the contour on MRI and the density of cystic lesions were examined.

Correlation of contour irregularity and clinical assessments

Correlations between parameters related to irregularity and the clinical score or the numbers of cystic lesions were analysed using Pearson's correlation coefficient with Statview 4.1 (Abacus, Berkeley, CA, USA). The p value was obtained from an analysis of variance, and statistical significance was defined as $p<0.05$.

Contour irregularity and clinical assessments of each K/L group

Post hoc test (Bonferroni/Dunn) was used for comparing contour irregularity and clinical assessments among each K/L group (Statview 4.1) where $p<0.05$ or 0.01 was considered significant.

Results

Interrater and intraobserver reliabilities

Interrater reliabilities were ATC=0.463, RUL=0.811, ASTC=0.384, and SDC=0.891. Intrarater reliabilities were ATC=0.573, RUL=0.834, ASTC=0.342, and SDC=0.923. (Measurements are defined in Materials and Methods.)

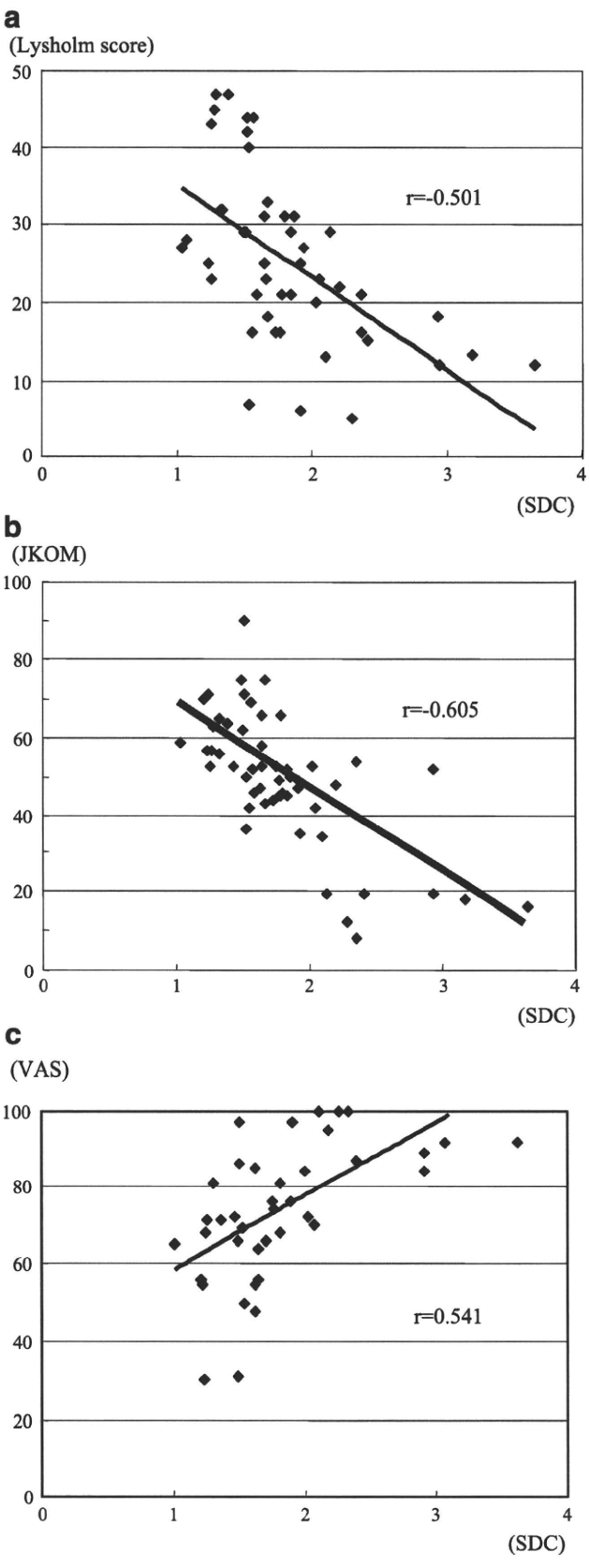

Fig. 2 Relationships between the standard deviation of the contour thickness (SDC) values and knee scores. The SDC scores are negatively correlated with **a** the Lysholm scores and **b** the Japanese Knee Osteoarthritis Measure (JKOM) scores, whereas **c** the SDC and visual analogue scale (VAS) are positively correlated

Therefore, the RUL and the SDC were selected for further analysis.

Clinical scores and X-ray grading

The average Lysholm score was 25.65±11.01 (range 5–47), the average VAS was 74.03±18.03 (range 30–100) and the average JKOM was 49.33±18.81 (range 8–90). Thirteen, seven, 23 and 12 knees were classified as K/L I, II, III and IV, respectively.

Correlations between clinical assessments and contour irregularity

1. RUL and knee Scores

The RUL values and Lysholm scores were negatively correlated ($r=-0.448$, $p=0.0016$), as were the RUL and the JKOM ($r=-0.623$, $p<0.0001$). A significant positive correlation was found between the RUL and the VAS ($r=0.472$, $p=0.0021$).

2. SDC and knee scores

The SDC values and the Lysholm scores were negatively correlated ($r=-0.501$, $p=0.0003$), as were the SDC and the JKOM ($r=-0.605$, $p<0.0001$). A significant positive correlation was found between the SDC and the VAS ($r=0.541$, $p=0.0003$; Fig. 2).

Contour irregularity and clinical assessments of each K/L group

The RUL tended to rise as the K/L grade increased, but no significant difference was observed between the K/L I and II and the K/L II and III. The SDC also tended to rise as the K/L grade increased, but no significant difference was observed between the K/L II and the K/L III. As for clinical assessments, the Lysholm score, VAS, and the JKOM tended to change according to the K/L grading, but only the K/L I and the K/L IV showed significant difference in all the three assessments (Table 1).

Correlation between MRI findings and histopathological examination

Derangements of the architecture of the trabeculae bones and cystic lesions were observed in the subchondral bone of the MFC in all nine cases used for histochemical

Table 1 Irregularities and clinical scores of each K/L grade

Average +/-standard deviation

	RUL	SDC	Lysholm score	VAS	JKOM
K/L I	1.08+/-0.05	1.16+/-0.33	35.9+/-10.2	66.3+/-18.4	60.1+/-7.1
K/L II	1.13+/-0.07	1.68+/-0.36	26.0+/-6.9	67.0+/-2.8	50.5+/-12.0
K/L III	1.16+/-0.07	1.73+/-0.48	22.8+/-10.7	71.6+/-19.1	50.9+/-21.5
K/L IV	1.31+/-0.13	2.52+/-0.78	20.2+/-6.1	86.8+/-10.9	36.6+/-16.2

(**: p<0.01, *: p<0.05, ns: not significant)

K/L Kellgren and Lawrence grade, *RUL* ratio of the upper surface to the lower surface of the contour, *SDC* standard deviation of contour thickness, *VAS* visual analogue scale, *JKOM* the Japanese Knee Osteoarthritis Measure

examinations, whereas less formation of cystic lesions was seen in the LFC. Average density of cystic lesions was 7.6± 4 .4/10 mm in the MFC and 1.6±1.6/10 mm in the LFC. Representative H&E staining of subchondral bone of the MFC is shown in Fig. 3a. Correlation coefficients for density of cystic lesions and irregularity were as follows: RUL: r=0.446, p<0.01; SDC: r=0.846, p<0.0001. Thus, irregular contours and the numbers of cystic lesions were positively correlated (Fig. 3-b).

Discussion

Obtaining a reliable index that objectively reflects knee OA severity should be helpful for determining treatment options and may possibly be useful to assess the efficacy of interventions. Evaluation based on imaging of affected joints is ideal, as it is not affected by the pathology of other joints that might obscure the results of an OA biomarker, such as in a urine or blood sample. Among several imaging technologies, radiographic examination is the most commonly used. However, the reliability for evaluating OA severity based upon radiographic findings is controversial.

Several studies showed that the radiographic features of knee OA were significantly associated with pain [12–14], whereas other studies have reported that OA severity based on radiographic findings was independent of pain [15, 16]. Many patients with relatively minimally damaged joints report knee pain [15]. In fact, we sometimes encounter a discrepancy between the characteristic findings of OA on X-ray and the clinical severity of knee OA. Recently, MRI has increasingly been used to diagnose or evaluate OA.

The typical features that may have an association with joint pain are osteophytes [17], bone oedema [4] and synovitis [4, 18, 19]. However, the clinical importance of these findings has not as yet been confirmed [20–22]. Oedema in the subarticular bone marrow adjacent to the knee detected by T2-weighted MRI is associated with painful knee OA [4]. In contrast, a finding on MRI of subchondral bone oedema cannot satisfactorily explain the presence or absence of knee pain [20].

In this study, we focused on the MFC contour, which presumably corresponds to the subchondral bone of the MFC on MRI [7]. One of the radiographic features of OA is a sclerotic change of subchondral bone. Sclerotic lesions are a mixture of thin and thick subchondral bone as OA becomes more severe. In our previous study, the cystic lesions of sclerotic lesions were positively stained with antibodies against pain-related molecules, including cyclooxygenase-2 (COX-2) and tumour necrosis factor alpha (TNF-α) [23]. Thus, we speculated that the subchondral bone of the affected compartment could be a source of pain, and that the extent of corresponding pathological changes that occurred in subchondral bone could be assessed by newly developed software presented in this paper.

Our previous pilot study showed that irregularity of the MFC on MRI was correlated with knee scores [8]. In this

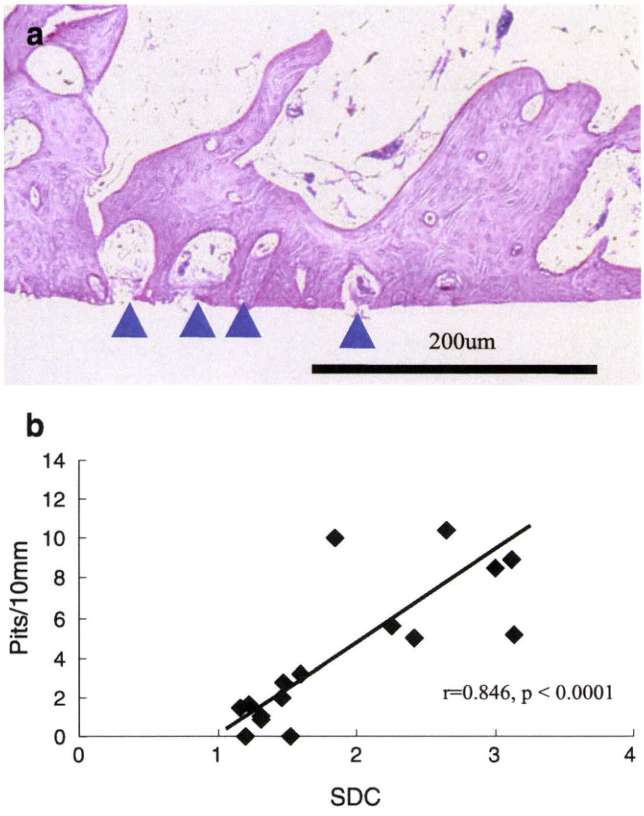

Fig. 3 Relationship between density of cystic lesions and irregularity. **a** Representative haematoxylin and eosin (H&E) staining of subchondral specimen retrieved at total knee arthroplasty (TKA) showed multiple formations of cystic lesions. **b** Density of cystic lesions and irregularity calculated according to preoperative magnetic resonance imaging (MRI) [standard deviation of the contour thickness (SDC)] are positively correlated

study, we present the possibility that RUL and SDC scores, which represent the irregularity of the MFC on MRI, could serve as indicators for disease severity in medial-type OA because the values of these two parameters increased as the Lysholm score and the JKOM decreased and as the VAS went up. Furthermore, these two parameters are positively correlated with the number of cystic lesions involved with the subchondral bone plate or the calcified zone. In this study, four parameters were initially employed, as the dependence upon only one or two values might miss detecting different types of irregular changes of the MFC. However, the ATC and the ASTC, which are related to changes in thickness, were far from being reliable. This was probably because a slight inconsistency in reproducing a black-and-white image during the process of conversion significantly affected these two parameters, especially the ASTC. We focused our attention on the femoral condyle and not on the tibial side in this study. There was a strong correlation between femoral and tibial cartilage volumes in the medial and lateral tibiofemoral joints both in subjects with normal knees and those with radiological OA [24]. Changes to the femur were sensitive enough, and for that reason, the femoral side was selected.

There are many methods for treating OA, from nonsurgical treatments such as nonsteroidal anti-inflammatory drugs, disease-modifying osteoarthritis drugs, rehabilitation and insoles, to surgical treatments such as arthroscopic debridement, osteotomy, arthrodesis, knee arthroplasty and others [25]. Choosing a treatment option is often difficult because there is no reliable objective index. Our next goal is to use this assessment system when selecting treatment options. For now, we can only say that when an irregularity of the MFC becomes large, TKA would be the only treatment, because a field of pain-generation area (i.e., COX-2 and TNF-α-positive subchondral bone area) will be removed at the time of TKA, so that treatments such as an arthroscopic technique or osteotomy to preserve these areas would fail. Further study will enable us to select suitable treatments based on the RUL and SDC values.

One of the limitations of this study relates to image accuracy. For high-quality image acquisition, three-dimensional techniques may be required, such as spoiled gradient-echo sequences [26] that would produce more reliable indices. Second, subjects in this study had apparent knee OA on X-ray. This technique is not useful for patients in the early stage of OA who only have cartilaginous damage and thus have no remarkable changes on X-ray. When evaluating these patients, other MRI protocols that can detect hyaline cartilage, such as T2 maps at 3 T [27] or contrast-material-enhanced techniques [26] have to be used. The problem with those methods is that they are too time consuming for daily clinical use where acquisition time is limited per patient. FSE proton density is the primary pulse sequence for MRI of the knee joint and is one of the suggested protocols in clinical work [28]. It only requires a short time for acquisition, so we routinely use those images in daily clinical work, and they were employed in this study.

Although MRI is a rather expensive investigation for assessment of OA severity, the assessment of contour irregularity could be a useful tool for patients when normal radiographs are not conclusive.

Conclusion

New computer software that assesses irregularity of the MFC contour is useful for evaluating medial-type OA knees. Objective values derived from this software are closely associated with knee scores and can be used as an indication for determining treatment options.